relaxed. Elastic relaxation law together with lateral confinement and erosion processes at surface conditions occurrence in rocks residual stresses when vertical uplift, what was marked at first time in [Goodman, 1989]. It has to be noted, if rocks would have Poisson elastic coefficient 0.5 (rubber), then elastic relaxation of gravitational stress state leads to equal decrement of both vertical and horizontal stresses, what actually happened in all modern computation of mantle convection.

Evaluations of the gravitational stress state energy are known $2.5 \cdot 10^{32}$ J. It is by three orders larger than kinetic energy of the planet and by four orders larger than energy of thermal convection. Our evaluations show that residual horizontal stresses of gravitational stress state (2/3 of lithostatic pressure and $\nu = 0.25$) compose circa half of total energy of elastic strains. This energy will relax through vertical convection movements causing additional (relative to ideal viscous fluid) plastic deformations, which *finally will be transitioned into heating*. Comparing the residual stress energy of unit volume released when uplifting from the core up to upper mantle boundary with the work spent on vertical transferring of this volume in thermal convection we will get $8 \cdot 10^9$ J и $3 \cdot 10^9$ J respectively. *Thus, energy confined in residual stress state is more than the energy spent on vertical uplift of unit volume*.

Therefore, our analysis has demonstrated that in all modern computations of thermal convection in the mantle in solutions is missing one of the most important components in energy balance — residual stress state conditioned by gravitational elastic-plastic compaction. In the presentation in the frames of traditional viscous model the problem will be posed and the solving equations followed from it, which take into account existence of the residual stresses in mantle and its impact on mantle convection will be given.

The research is supported by RFBR grant 09—05—01213a.

References

Dinnik A. N. About rock pressure and calculation column of circle mine // Ingeniring worker. — 1926. — № 3. — P. 1—12 (in Russian).

Goodman R. E. Introduction to rock mechanics. (2nd Edition). — New York: John Wileyand Sons, 1989. — 583 p.

Jager J. C. Elasticity Fracture and Flow. — London: Methuen and Co. LTD, 1962. — 208 p.

Nikolaevsky V. N. Geomechanics and fluid dynamics. — Moscow: Nedra, 1996. — 446 p. (in Russian).

Rebetsky Yu. L. Mechanism of tectonic stress generation in the zones of high vertical movements // Fiz. Mezomekh. — 2008. — **11**, № 1. — P. 66.

Rebetskii Yu. L. Possible mechanism of horizontal compression stress generation in the Earth's crust // Doklady Earth Sciences. — 2008. — **423A**, № 9. — P. 1448—1451.

Trubitsyn V. P. Equations of termal convection for uncompressibility viscous mantle with phase transition // Phys. Earth. — 2008. — № 12. — P. 83—91 (in Russian).

Seasonal variation of induction vectors

© I. Rokityansky[1], T. Klymkovich[2], V. Babak[1], T. Savchenko[1], 2010

[1]Institute of Geophysics, National Academy of Sciences of Ukraine, Kiev, Ukraine
rokityansky@gmail.com
[2]Carpathian Branch of Institute of Geophysics, National Academy of Sciences of Ukraine, Lvov, Ukraine
tamara@cb-igph.lviv.ua

In the geoelectromagnetic studies of electrical conductivity of the Earth's interior, the response function (RF) is supposed to be any function (impedance, apparent resistivity, induction arrow, horizontal MV tensor…) derived from the Earth's electromagnetic (EM) data which provides us with possibility to determine the conductivity structure in the Earth. Ideally RF depends only on the Earth's conductivity and does not depend on the properties of external EM field used.

Widely used RF for EM monitoring is induction vector **C**:

$$\mathbf{C} = Ae_x + Be_y \,, \qquad (1)$$

where e_x and e_y are unit vectors, x — is pointed to

North, y — to East, z — downward, A and B form a 1×2 matrix which transforms the horizontal magnetic field (B_x, B_y) observed at a station into the vertical component B_z

$$B_z = AB_x + BB_y \ . \qquad (2)$$

In (1), (2) all quantities are complex and depend on period T of variations, thus supposing that we deal with observed magnetic field $\mathbf{B}(T)$ after harmonic (Fourier) analysis of total field.

The real $\mathbf{C} = A_u e_x + B_u e_y$

and imaginary $\mathbf{C}_v = A_v e_x + B_v e_y$

parts of the vector **C** are referred to as the real and imaginary Wiese (or Parkinson) induction vectors or arrows.

Real induction arrows possess an important property: in the notation of Wiese, they are directed away from good conductor, in Parkinson's notation — to good conductor.

Really observed $\mathbf{B}(T)$ is composed of

$$\mathbf{B}(T) = \left(\mathbf{B}_{en} + \mathbf{B}_{in} + \mathbf{B}_{ia}\right) + \mathbf{B}_{noise} + \mathbf{B}_{LE} \ , \qquad (3)$$

where: $\mathbf{B}_{en}$ — normal external primary magnetic field (of period T) of the currents in ionosphere and magnetosphere; $\mathbf{B}_{in}$ — normal internal secondary magnetic field of the currents induced in hypothetical horizontally layered (1D conductivity) Earth; $\mathbf{B}_{ia}$ — anomalous secondary field arising on local/regional conductivity anomaly as result of re-distribution of the currents responsible for $\mathbf{B}_{in}$.

For commonly used in magnetotellurics idealized model of Tikhonov — Cagniard (plane wave vertically incident on horizontally layered Earth) the normal field in (3) has only horizontal components x and y, B_z in (2) is purely anomalous. If two last terms in (3) can be neglected, the [A, B] matrix and induction vector carry pure information on conductivity anomaly. And if induction vector varies with time one can suppose that conductivity structure changes.

In reality, at least 3 more factors can vary RF, so RF variation with time can be caused by 1) variation of the properties of external source field i.e. by its deflection from T—C model, 2) noise, 3) superposition of transient internal EM fields — lithospheric emission (LE). The latter cause together with the change of lithosphere electrical conductivity manifest geodynamic processes including earthquake (EQ) and volcano activity preparation and are of great interest. Variability of TF was reported many times during last 50 years including two reviews of early studies by Niblett and Honkura, 1980 and Kharin, 1982. After transition to geomagnetic field digital registration, reliability of TF study was essentially improved.

From common considerations we can suppose that EQ and volcano eruption precursors should have an aperiodic temporal regime appearing once or several times before EQ. Then, regular periodic TF variations can be treated as a background for the precursors study.

Annual (or seasonal) variation of **C** components were presented in works [Fujita, 1990; Moroz Yu., Moroz T., 2006; Moroz et al., 2006; Korepanov, Tregubenko, 2009]. Consider their results.

In Fig. 1 the results of induction vectors study in Japan is presented. Annual variation appears most clearly at the northern component in Kakioka (KAK) observatory where real vector attains maximum at the period 50 m and imaginary one change its sign [Shiraki, Yanagihara, 1975]. In Fig. 1, *d* (averaged for 13 years monthly mean data), annual variation is clearly seen especially at long periods where it exceeds error given by vertical bars. A_v changes its level according frequency response of C_v. Fig. 1, *c* shows long term trend which can be related with EQ occurrence, in particular, with Kanto EQM7.8 in 1923.

Fig. 2 presents the results of three years monitoring in Kamchatka. C_u exhibits highly interesting behavior: at the shortest period 250 s, annual variation is maximal 0.1/half year with minimum in summer season, at longest period 6000 s the variation equals 0.05/half year with maximum in summer season. At the periods 1000 and 3000 s the variation is small. Quite different behavior exhibits C_v (Fig. 2, *c*). Analysis of frequency characteristic (Fig. 2, *b*) together with geoelectric structure of the region give ground for attempt to explain RF behavior.

Fig. 3 displays annual variation only for Patrony observatory where it attains almost 0.1/half year at long and short periods and reduces in 3 times at periods around 1000 s where C_u attains maximum (Fig. 3, *b*). Sign of variation does not change. In Enhaluk observatory annual RF variation does not exceed 0.02 and does not seen in the noise.

V. I. Tregubenko during more than 10 years drives MV monitoring in Ukraine. He applayed best processing program and developed reliable monitoring processing procedure for EQ prediction and also received annual RF variations. According his opinion these variations can be seen most clearly in phase (Fig. 4).

Conclusion.

1. Annual (or seasonal) variation of induction vector components really exists and in some cases has rather pronounced magnitude.

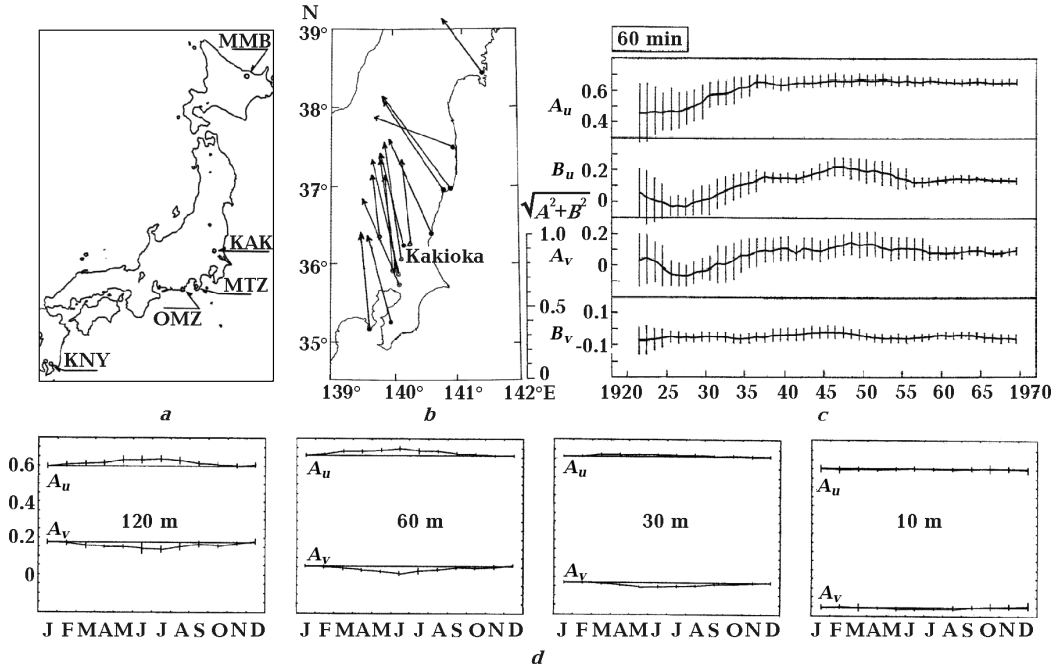

Fig. 1. Results from Japan: *a* — Observatories position; *b* — $\mathbf{C}_u$ in central Japan for T=15÷60 m [Kuboki, 1972]; *c* — ten years running averages of **C** components in Kakioka for the period 60 m, vertical lines show 95 % confidence intervals [Shiraki, Yanagihara, 1977]; *d* — seasonal variation given by monthly means of 1976—1988 Kakioka data for four periods.

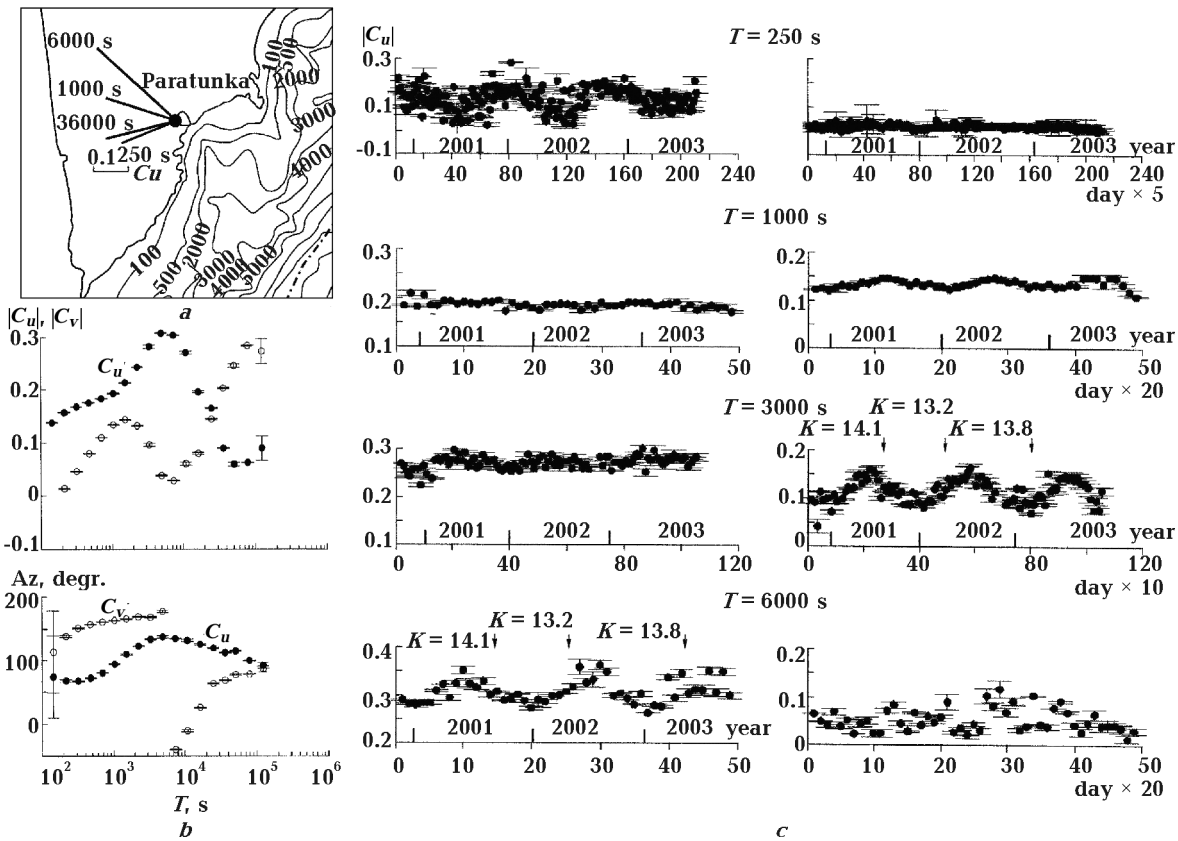

Fig. 2. Results from Kamchatka [Moroz et al., 2006]: *a* — $\mathbf{C}_u$ (Wiese convention) at four periods on South Kamchatka map with Pacific bathymetry lines marked in meters; *b* — modulus and azimuth of $\mathbf{C}_u$ and $\mathbf{C}_v$ versus period for Paratunka observatory; *c* — three years monitoring of $\mathbf{C}_u$ and $\mathbf{C}_v$ with averaging 5, 10 or 20 days (which indicated at horizontal axis legend) at four periods. Arrows show the time of strong (K>13) EQs at the distance 150 km or less from Paratunka observatory.

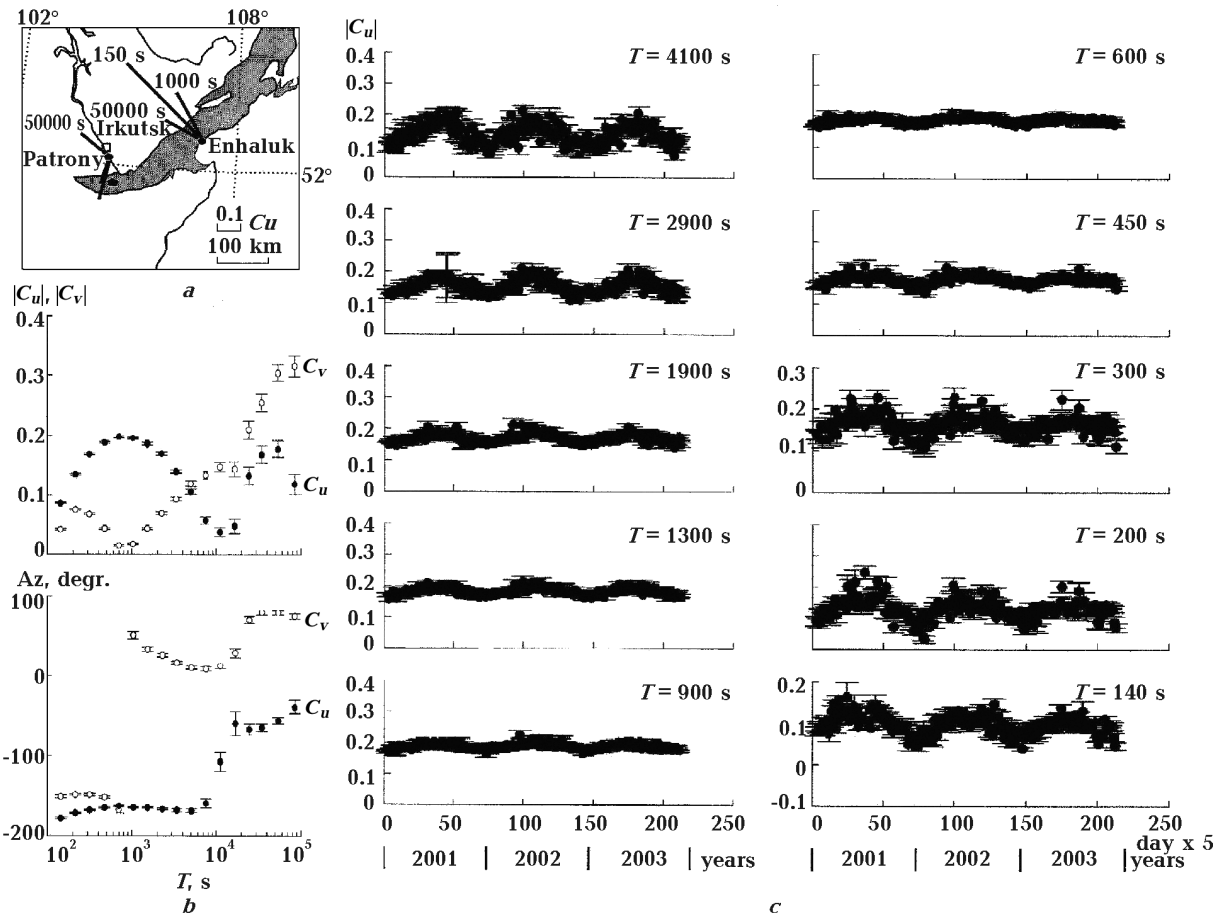

Fig. 3. Baykal rift [Moroz Yu., Moroz T., 2006]: *a* — real induction vectors (Parkinson convention) for two observatories for three periods; *b* — modulus and azimuth of $\mathbf{C}_u$ versus period for Patrony observatory; *c* — three years monitoring of $\mathbf{C}_u$ with averaging 5 days at ten periods.

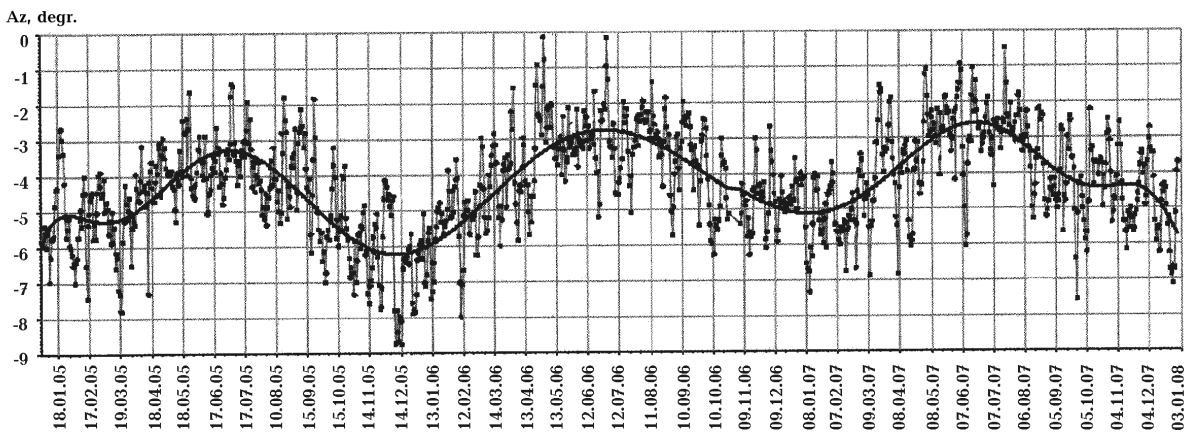

Fig. 4. Phase of the tipper meridional component (arg A) variation at T=1000 s in Blue Bay (South Crimea) Each point is duirnal arg A value after averaging in 5 days window [Korepanov, Tregubenko 2009]

2. In looking for EQ precursors (supposing be aperiodic) annual variation should be well studied and reduced.

3. Causes of annual variation may be a) the change of electrical conductivity in the Earth's interior, forming induction vectors; b) seasonal variation of the external source parameters leading to deflection from T—C model. c) superposition of seasonally variable parts of the last terms in equation (3).

References

Fujita S. Monitoring of Time Changes of Conductivity Anomaly Transfer Functions at Japanese Magnetic Observatory Network // Memoirs of the Kakioka magnetic observatory. — 1990. — **23**, № 2. — P. 53—87.

Korepanov V. E., Tregubenko V. I. Features of construction and trends of modern instruments development for magnetotelluric and magnetovariational soundings // Geophys. J. — 2009. — **31**, № 4. — P. 181—190 (in Russian).

Kuboki T. The Anomaly of Geomagnetic Variation in Japan (Part V) // Memoirs of the Kakioka magnetic observatory. — 1972. — **15**, № 1. — P. 63—80 (in Japanese).

Moroz Yu. F., Moroz T. A. Magnetovariational studies in the Baykal lake region // Fizika Zemly. — 2006. — № 11. — P. 93—98 (in Russian).

Moroz Yu. F., Smirnov S. E., Moroz T. A. The results of monitoring of geomagnetic field variations in Kamchatka // Fizika Zemly. — 2006. — № 3. — P. 49—56 (in Russian).

Shiraki M., Yanagihara K. Transfer Functions at Kakioka (Part I) // Memoirs of the Kakioka magnetic observatory — 1975. — **16**, № 2. — P. 143—155 (in Japanese).

Shiraki M., Yanagihara K. Transfer function at Kakioka (Part II). Reevaluation of Their Secular Changes // Memoirs of the Kakioka magnetic observatory. — 1977. — **17**, № 1. — P. 19—25 (in Japanese).

High Rayleigh Number Mantle Convectionon GPU

© D. Sanchez[1], D. Yuen[1], G. Wright[2], G. Barnett Jr.[3], 2010

[1]Minnesota Supercomputing Institute, University of Minnesota, USA
[2]Departament of Mathematics, Boise State University, USA
[3]Departament of Applied Mathematics, University of Colorado, Boulder, USA

The performance, potential growth, availability, and affordability of GPUs has made them attractive to scientists for many years. Although historically cumbersome and difficult to use for scientific software, the introduction and refinement of high-level development tools, such as CUDA, have made GPU computing accessible. With the advent of architectures, such as NVIDIA's Fermi, which explicitly cater to scientists by enabling more memory, faster access to that memory, and better double-precision support than ever before, members of the computational world are finding GPU difficult to ignore.

Using finite-difference methods with second-order accuracy in space and third-order accuracy in time, we investigate 2D and 3D thermal convection at the infinite Prandtl number limit, at resolutions on the order of 1000×2000 2D and 400×400×200 3D grid points. Our CUDA code makes extensive use of

Fig. 1. Performance scaling with grid size on Tesla C1060.